

Incorporating Fault Intensity and AVO Inversion to Characterize a Shale Gas Reservoir

Carl Reine*, Nexen Inc., Calgary, Alberta, Canada

carl_reine@nexeninc.com

and

Sean Lovric, Nexen Inc., Calgary, Alberta, Canada

Summary

We show that fault intensity and AVO inversion show insights into hydraulic fracturing operations. This is supported by microseismic data using calculations of event density, b-value, and D-value. Production data is also shown to support these conclusions. We also demonstrate that fault intensity is linked to the azimuthal anisotropy of the AVO inversion. This helps both infer the presence of faults that are below seismic imaging resolution, and potentially determine the spatial scale at which anisotropy measurements relate to natural faults and fractures.

Introduction

One of the key contributions that geophysics can make to the development of shale gas plays is to explain and predict the behaviour of hydraulic fracturing operations and the resulting gas production. To accomplish this, we look at the relationship between microseismic and surface seismic calculations.

Surface seismic is used to determine the underlying rock properties of the shale reservoir. Prestack AVO inversion allows seismic amplitudes to reveal useful mechanical properties such as Poisson's ratio and Young's modulus. These values can then be used to determine a measure of reservoir brittleness (Rickman, 2008). When extended to different azimuthal sectors, the anisotropy of the inverted results can be used as an indicator of natural fracturing (Bakulin et al., 2000) or local stress changes (Gray et al., 2012).

For hydraulic fracturing, microseismic data contains both spatial information and attribute information revealing the conditions under which the events are occurring. Spatially, event density is a useful display of how microseismic energy is concentrated, and D-values (Grob & van der Baan, 2011) describe the spatial distribution of events, indicating the spread in the total microseismic cloud. The distribution of microseismic magnitudes can be characterized by the b-value (Gutenberg & Richter, 1954), offering insight to the mechanism of failure (Wessels et al., 2011).

Here we show the applicability of the above measurements in the Horn River basin. We show examples where brittleness and fault intensity determine the density of microseismic events from hydraulic fracturing. The naturally occurring fractures also drive the microseismic b-values, likely due to the change in failure characteristics. Furthermore, we show how the seismic-scale fracturing is related to the azimuthal anisotropy of the AVO inversion, and discuss a strategy for calculating stress and stress anisotropy from this information. Finally, we show how brittleness and fault intensity have an effect on the gas production of the hydraulically fractured wells.

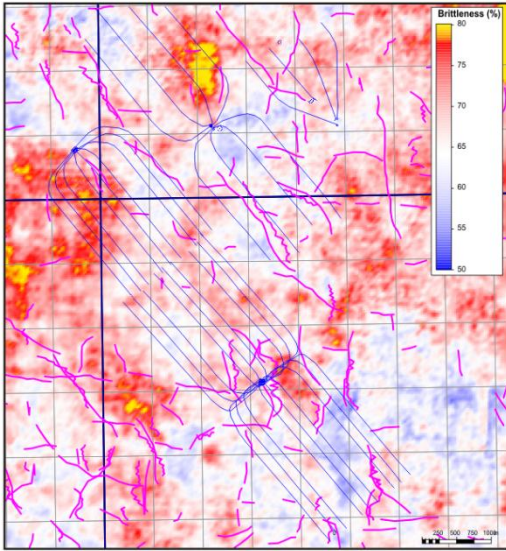


Figure 1: Median brittleness, a function of Young's modulus and Poisson's ratio, mapped for the lowermost zone in the reservoir. Seismic-scale faults are indicated in magenta.

Method

Fault intensity is calculated from an analysis of the directly-observed and inferred seismic-scale discontinuities, as detailed by Reine & Dunphy (2011). In map view, these faults are modelled as linear features, which allows for measurements of azimuth, length, and intensity (cumulative length per unit area). The intensity calculations are made over a 500 m x 500 m cell, which rolls in increments of 100 m.

A simultaneous AVO inversion (Hampson et al., 2005) is performed to obtain P-impedance, S-impedance, and density. These values are combined to produce

volumes of Young's modulus, Poisson's ratio, and brittleness B quantified using the Rickman (2008) relationship

$$B = \frac{1}{2} \left(\frac{E - E_{\min}}{E_{\max} - E_{\min}} + \frac{\nu - \nu_{\max}}{\nu_{\min} - \nu_{\max}} \right) \cdot 100. \quad (1)$$

Here E and ν are Young's modulus and Poisson's ratio respectively, and the minimum and maximum values of these parameters are taken from the zone being characterized.

Four mechanical layers are seen in the data that correspond to geological boundaries. Using a 3D geological model, we first convert the geological layers into time, and then snap them to the transitions between mechanical layers on the Poisson's ratio volume. This allows for representative values in each layer to be calculated and mapped (Figure 1).

The same initial model and inversion parameters used for the above data are then applied to an inversion of gathers processed into four azimuthal sectors. Once mechanical properties are calculated, a function of the form

$$z(\phi) = A + B \cos[2(\phi - \phi_0)] \quad (2)$$

is fit to the median maps z for P-impedance and Poisson's ratio for each azimuth ϕ (Figure 2). This fit employs a non-linear inversion using the Gauss-Newton method (Aster et al., 2005). The background value A is checked with the full-azimuth inversion results for consistency. The ellipticity B provides a measure of the magnitude of azimuth anisotropy, along with dominant direction ϕ_0 .

Microseismic data was recorded for the hydraulic fracturing operations on a number of wells. To characterize the data spatially, the events were assigned to one of the four mechanical units using the 3D geological model. This allowed the events to be summarized as a density display for each layer. The density was calculated as the number of events in a 100 m x 100 m cell. Spatial properties were also measured by first determining the separation between each pair of microseismic events. The slope of the linear region on a log-log plot of cumulative events versus separation is then used to calculate the D-value. Using a similar method, the microseismic b-value was also determined for each hydraulic fracture stage on a plot of cumulative events versus maximum magnitude.

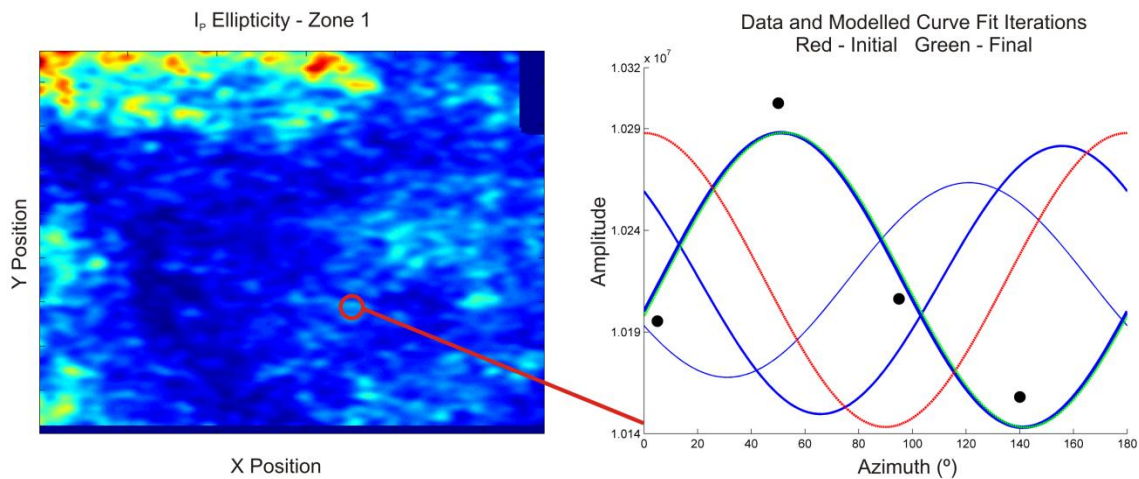


Figure 2: Example fit of the $z(\phi) = A + B \cos[2(\phi - \phi_0)]$ function to azimuthal P-impedance data in the uppermost zone. The map on the left shows the spatially filtered ellipticity values. The curve fit determining the value at the circled point is shown on the right, along with the data points at all four azimuths. Five model iterations are shown, with the final curve shown in green.

Analysis

The relevance of seismic-scale faults is that natural fractures are expected to display a predictable scale relationship, often a power-law, between large and small features (Bonnet et al., 2001). The smaller microseismic failure radii, calculated using a Brune model (Brune, 1970), align with the same scale relationship as determined by seismic faults. This is consistent with the idea that hydraulic fractures, and the microseismic events that they cause, occur largely by reactivation of natural features. The calculated fault intensity is also closely correlated to the fracture count from an FMI log in a horizontal well, supporting that large-scale faults are associated with an increase in small-scale fracturing.

However fault intensity, which here is based on the ability to resolve (or at least infer resolution of) discontinuities, does not completely characterize a reservoir. The mechanical properties of the rock are also an important factor. Figure 3 shows a plot of microseismic event density versus seismic fault intensity, with points coloured by brittleness. These data are specific to a single geomechanical zone in the reservoir. Two peaks in event frequency can be seen, the first corresponding to the highest fault intensity. The second peak, while at a lower fault intensity, has the highest brittleness values, showing that both factors control the location of microseismic events.

Event magnitudes are also affected by the reservoir properties. Figure 4 shows a grid of microseismic b-values based on calculations for individual stages, which is overlaid by the discrete fault events that contribute to the fault intensity map. The regions where faults are present consistently show lower b-values, suggesting that these events are dominated by natural-fault reactivation (Maxwell et al., 2009). Similar conclusions can be shared from the microseismic D-values, which show that in the region of natural faulting, the events in the microseismic clouds have greater separations.

Ellipticity maps of P-impedance and Poisson's ratio both show similar behaviour to one another. Spectral analysis of the maps in the spatial frequency domain shows that three dominant bandwidths are evident. The high spatial frequency component (wavelengths < 200 m) is dominated by noise, and is filtered out for mapping purposes, leaving low-frequency (wavelengths > 1000 m) and mid-frequency components. The mid-frequency component matches well with the scale of observed natural faulting, and we suggest that this might be a useful criterion for identifying fracture anisotropy effects separate from background changes in stress anisotropy.

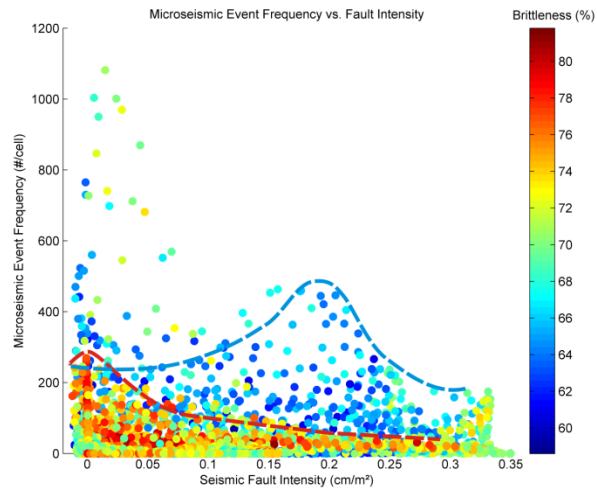


Figure 3: Microseismic event density versus seismic fault intensity coloured by brittleness. Two trends of high event densities occur with either high fault intensities, or high brittleness values.

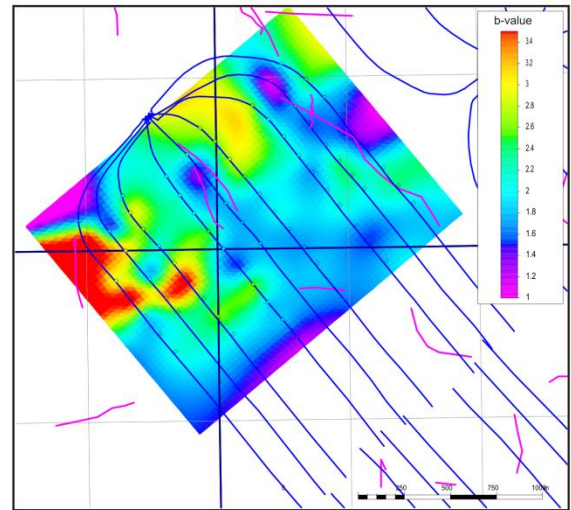


Figure 4: Microseismic b-values calculated for individual stages and gridded. Seismic-scale faults and positive curvature features are overlaid in magenta. The lowest b-values correspond to the location of natural fractures.

We also find that production results correlate with the fault intensity, brittleness, and azimuthal anisotropy. For nine wells in the zone of analysis, the highest producers occur in regions with higher brittleness, higher fault intensity, and lower azimuthal anisotropy. While this last point may be counter intuitive, a possible explanation is that the single fracture set assumption in equation 2 is invalid, and there may be two or more sets, making the four azimuthal sectors appear more isotropic.

Conclusions

Predicting the behaviour of a shale-gas reservoir is an ambitious goal with great value. While we are not suggesting that seismic data alone is able to provide all of the necessary characterization, we have shown that some valuable information is nevertheless available. By observing the seismic-scale faults on the seismic image, and by calculating the reservoir's mechanical properties through AVO inversion, we are able to validate observations from microseismic and production data.

In our examples, hydraulic fractures tend to produce the most microseismic energy in areas with high fault intensity, followed closely by areas with high brittleness. The natural faults also affect the distribution of the microseismic cloud and the magnitude of the events. Finally, while gas production is a complicated process, the highest gas production of the analyzed wells comes from wells with higher brittleness, higher fault intensity, and lower azimuthal anisotropy.

Acknowledgements

A large number of people have been involved in the everyday operations that have contributed to this work, from data collection and processing to geological modelling and production analysis. We would like to thank Nexen's shale gas team for their efforts, and thank Nexen for allowing us to show these results.

References

- Aster, R.C., B. Borchers, C.H. Thurber, 2005, Parameter estimation and inverse problems, Elsevier Academic Press, volume **90** of International Geophysical Series.
- Bakulin, A., V. Grechka, and I. Tsvankin, 2000, Estimation of fracture parameters from reflection seismic data - Part I: HTI model due to a single fracture set: *Geophysics*, **65**, 1788-1802.
- Bonnet, E., O. Bour, N.E. Olding, P. Davy, I. Main, P. Cowie, and B. Berkowitz, 2001, Scaling Of Fracture Systems In Geological Media: *Reviews of Geophysics*, **39**, 347-383.
- Brune, J.N., 1970, Tectonic stress and the spectra of seismic shear waves from earthquakes: *Journal of Geophysical Research*, **75**, 4997-5009.
- Gray, D., P. Anderson, J. Logel, F. Delbecq, D. Schmidt, and R. Schmid, 2012, Estimation of stress and geomechanical properties using 3D seismic data: *First Break*, **30**, no. 3, 59-68.
- Gutenberg, R., and C.F. Richter, 1954, *Seismicity of the earth and associated phenomena*, 2nd ed.: Princeton University Press.
- Hampson, D.P., B.H. Russell, and B. Bankhead, 2005, Simultaneous inversion of pre-stack seismic data: 75th Annual Meeting, SEG, 1633-1637.
- Maxwell, S.C., M. Jones, R. Parker, S. Miong, S. Leaney, D. Dorval, D. D'Amico, J. Logel, E. Anderson, and K. Hammermaster, 2009, Fault activation during hydraulic fracturing: 79th Annual Meeting, SEG, 1552-1555.
- Reine, C., and R. Dunphy, 2011, Weighing in on the seismic scale: The use of seismic fault measurements for constructing discrete fracture networks in the Horn River basin: 2011 CSPG/CSEG/CWLS Convention, CSPG/CSEG/CWLS.
- Rickman, R., M. Mullen, E. Petre, B. Grieser, and D. Kundert, 2008, A practical use of shale petrophysics for stimulation design optimization: All shale plays are not clones of the Barnett shale: Annual Technical Conference and Exhibition, SPE, SPE115258.
- Wessels, S.A., A De La Pena, M. Kratz, S Williams-Stroud, and T. Jbeili, 2011, Identifying faults and fractures in unconventional reservoirs through microseismic monitoring: *First Break*, **29**, no. 7, 99-104.